



Article

Double Substituted with Manganese and Strontium Tricalcium Phosphate Coatings on Zinc-Lithium Biodegradable Alloys for Biomedical Implant Applications

Julietta V. Rau 1,*, Angela De Bonis 2, Roberto Teghil 2, Mariangela Curcio 2, Inna V. Fadeeva 3, Katia Barbaro 4, Massimo Di Menno Di Bucchianico 1, Marco Fosca 1 and Yufeng Zheng 5

- Istituto di Struttura della Materia, Consiglio Nazionale delle Ricerche (ISM-CNR), Via del Fosso del Cavaliere 100, 00133 Rome, Italy
- ² Dipartimento di Scienze, Università della Basilicata, Via dell'Ateneo Lucano 10, 85100 Potenza, Italy
- 3 A.A. Baikov Institute of Metallurgy and Material Science, Russian Academy of Sciences, Leninsky 49, Moscow 119334, Russia
- Istituto Zooprofilattico Sperimentale Lazio e Toscana "M. Aleandri", Via Appia Nuova 1411, 00178 Rome, Italy
- 5 School of Materials Science and Engineering, Peking University, No.5 Yi-He-Yuan Road, Hai-Dian District, Beijing 100871, China
- * Correspondence: giulietta.rau@ism.cnr.it

Abstract: To address the clinical needs for biodegradable implant materials, in this work, zinc-lithium (Zn-Li) biodegradable alloy was coated with double-doped manganese and strontium resorbable tricalcium phosphate (Mn,Sr-TCP). The Pulsed Laser Deposition method was applied for coating preparation. For coating characterization, Fourier Transform Infrared Spectroscopy, X-ray Diffraction, Scanning Electron Microscopy coupled with Energy Dispersive X-ray, and X-ray Photoelectron Spectroscopy were used. The microbiology experiments were performed, testing the inhibition of growth of Gram-positive (*Staphylococcus aureus*, *Enterococcus faecalis*) and Gram-negative (*Salmonella typhimurium*, *Escherichia coli*) bacteria strains and *Candida albicans* fungus. The obtained results evidenced about 10% of inhibition of all four bacteria strains by the Mn,Sr-TCP-coated Zn-Li samples, exerting the most pronounced effect on *C. albicans* fungus (about 50% of inhibition of growth). The prepared coatings can be useful for improving the degradation behavior and biological characteristics of Zn-Li alloys.

Keywords: coatings; biodegradable coatings; tricalcium phosphate coatings; manganese and strontium substituted tricalcium phosphate; manganese- and strontium-doped tricalcium phosphate; biodegradable alloys; Zn-Li alloy

Citation: Rau, J.V.; De Bonis, A.;
Teghil, R.; Curcio, M.; Fadeeva, I.V.;
Barbaro, K.; Di Menno Di
Bucchianico, M.; Fosca, M.; Zheng,
Y. Double Substituted with Manganese and Strontium Tricalcium Phosphate Coatings on Zinc-Lithium Biodegradable Alloys for Biomedical
Implant Applications. *Coatings* 2023,
13, 36. https://doi.org/10.3390/
coatings13010036

Academic Editor: Seunghan Oh

Received: 22 November 2022 Revised: 21 December 2022 Accepted: 23 December 2022 Published: 25 December 2022



Copyright: © 2022 by the authors. Licensee MDPI, Basel, Switzerland. This article is an open access article distributed under the terms and conditions of the Creative Commons Attribution (CC BY) license (https://creativecommons.org/licenses/by/4.0/).

1. Introduction

Over the last two decades, biodegradable metals have emerged as promising materials for various biomedical implant devices, having the scope to reduce the use of permanent metallic implants made of stainless steel- or titanium (Ti)-based alloys and, consequently, to avoid implant removal surgeries and significantly reduce the costs. Biodegradable metals are promising for such applications as bone implants, cardiovascular stents, etc. [1]. Among the advantages of biodegradable metals are their biocompatibility and degradation characteristics, while among the problems to be solved are their low mechanical properties for load-bearing bone substitute applications and their corrosion performance, which is too high to match the healing rate of the host bone tissue. Some biodegradable metals are already in use in clinics. Bone screws made from biodegradable magnesium (Mg)-based alloys possess better mechanical properties than those made of biodegradable polymers, they are approved for clinical use by the Conformité Européene

Coatings 2023, 13, 36 2 of 13

(CE) and the Korea Food and Drug Administration (KFDA), respectively [2,3], and clinical trials in other countries are on the way [4]. However, there is still a gap between the mechanical properties of biodegradable materials such as polymers and Mg-based alloys compared to traditional permanent metal implants, and, therefore, their use is limited to non-load-bearing applications. Recent achievements in biodegradable zinc (Zn)-based materials produced alloys with outstanding mechanical strength. Furthermore, Zn plays an important role in bone metabolism, stimulating osteoblast bone formation and inhibiting osteoclast differentiation [5,6]. Therefore, biodegradable Zn-based alloys appear promising to meet the clinical needs in orthopaedics [7].

One of the most effective ways to improve the properties of a biodegradable metal surface, to reduce and control the degradation behavior, and to improve the surface biocompatibility is to coat it with bioactive glasses or biomimetic calcium phosphates [8–11]. Tricalcium phosphate (TCP) is a resorbable bioceramic; β -tricalcium phosphate (β -TCP) is one the most used synthetic bone grafts due to being osteoconductive and osteoinductive [12]. In order to modulate and further boost the osteoinductive ability of β -TCP, the incorporation of metal ions is performed. Previous studies demonstrated that metal ions could be easily introduced into the β -TCP structure by substitution in Ca²⁺ positions [13]. Essential ions, such as strontium (Sr²⁺) [14,15], copper (Cu²⁺) [16], magnesium (Mg²⁺) [17], manganese (Mn²⁺) [18,19], iron (Fe²⁺) [11], zinc (Zn²⁺) [20], etc., can enhance the biological performance of β -TCP and induce osteo- and angiogenesis. Moreover, Cu²⁺ [16], Mn²⁺ [18], Fe²⁺ [11], and Zn²⁺ [20] are known to have antimicrobial properties.

It should be noted that implant-related infections are among the main reasons for implant failure, with associated high economic and social costs. The prevention of biomaterial-associated infections should specifically focus on the inhibition of both bacterial adhesion and biofilm formation. Unacceptably high rates of septic complications, especially in high-risk patients and procedures, are reported in [21,22]. In order to make the implant surface antibacterial and prevent infections, it is possible to coat it with materials possessing antibacterial characteristics, among them Cu, Mn, Fe, and Zn-substituted calcium phosphates.

Multiple substitutions of hydroxyapatite (HA) containing Mg²⁺, Mn²⁺, and Sr²⁺ ions were reported in [23]. In that study, authors investigated the possibility of increasing the number of foreign ions doping in HA structure by a co-substitution with other elements to enhance the structural stability of HA and, in particular, with Sr2+ ions. Scaffolds for bone regeneration based on β-TCP incorporating Sr, Zn, and Mn were successfully developed in [24]. Sr and Mn co-substituted HA ceramic coatings were deposited on Ti using a cathodic electrodeposition method [25]. The authors [25] showed that the MC3T3-E1 cells exhibited better morphology, adhesion, spreading, proliferation, and expression of alkaline phosphatase on the SrMn-HA surface compared to pure HA. In our previous study, double substituted Sr²⁺, Mn²⁺ β-TCP powder was synthesized, and its antibacterial properties were studied [26]. It was established that single phase Ca_{3-2x}(M´M´´)_x(PO₄)₂ solid solutions are formed only at $x \le 0.286$, where M' and M''—divalent metal ions, such as Zn²⁺, Mg²⁺, Cu²⁺, Mn²⁺, and that in case of double substitutions, the incorporation of Sr²⁺ ions allows one to extend the limit of solid solution due to the enlargement of the unit cell structure. It was also reported that antimicrobial properties depend on the substitution ion occupation of Ca^{2+} crystal sites in the β -TCP structure. The combination of two different ions in the Ca5 position, on one side, and in the Ca1, Ca2, Ca3, and Ca4 positions, on another side, significantly boosts antimicrobial properties [26].

In the present work, for the first time, zinc-lithium (Zn-Li) alloys were coated with a double substituted with Mn^{2+} and Sr^{2+} ions β -TCP, with the scope to promote osteoinductive effect and to impart antimicrobial properties. Sr is known to influence the bone balance towards osteosynthesis, stimulating new bone formation and inhibiting bone resorption [27–29]. It has been used for a long time in osteoporotic therapies. The authors [30] studied the effect of Sr on human osteoblasts and, namely, on their viability, proliferation, cell morphology, protein production, and protein activity and concluded that Sr has a

Coatings 2023, 13, 36 3 of 13

positive effect on bone formation. In ref. [18], the biological effects of Mn-doped β -TCP were studied, reporting that the inhibition of the growth of several bacterial species was observed to be more effective against Gram-positive bacteria rather than against Gram-negative ones without imparting cytotoxicity. Moreover, Mn is an essential micronutrient for living bodies; its amount in mammals is about ~1.5 μ g Mn per g of tissue weight, and about 1–9 mg daily for human adults is considered acceptable [31]. Additionally, Mn is involved in bone formation and metabolism of amino acids, carbohydrates, and cholesterol [32].

Therefore, the goal of this study was to improve the properties of Zn-Li biodegradable alloys by coating them with double-doped Mn,Sr- β -TCP. The Pulsed Laser Deposition (PLD) method was applied as the coating's deposition technique. Numerous methods were proposed to deposit bioactive thin films. Among physical deposition techniques, laser-assisted methods allow the depositing of inorganic [33] and composite [34] films, controlling the film thickness, crystallinity, and morphology by varying deposition parameters, such as laser wavelength and pulse duration, substrate temperature, and gas buffer. Briefly, the mechanism of nanosecond laser ablation can be described considering that during the interaction of a laser pulse with a solid target, the vaporization of the solid phase takes place [35,36]. Following this, the formation and expansion of an ionized plasma, whose composition reflects the target stoichiometry, can be observed. When the plasma arrives on the substrate surface, a film starts to grow due to the coalescence of clusters and droplets. It was shown that films deposited using PLD present good adhesion strength and hardness and are characterized by a rough surface [33,34].

In the present work, for coatings characterization, Fourier Transform Infrared Spectroscopy (FTIR), X-ray Diffraction (XRD), and Scanning Electron Microscopy (SEM) coupled with Energy Dispersive X-ray (EDX) and X-ray Photoelectron Spectroscopy (XPS) were used. The microbiology tests of the prepared coated Zn-Li alloys were performed with the Gram-positive (Staphylococcus aureus (S. aureus), Enterococcus faecalis (E. faecalis)) and Gram-negative (Salmonella typhimurium (S. typhimurium), Escherichia coli (E. coli)) bacteria strains and Candida albicans (C. albicans) fungus.

2. Materials and Methods

2.1. Zn-Li Alloy Preparation

A Zn-0.4 wt.% Li alloy ingot was prepared from a Zn (99.99%) and Zn-Li master alloy (6 wt.% Li) ingot by the Hunan Rare Earth Metal Material Research Institute of China (Changsha, China). A cast iron mold with ZnO coating was used for casting. The resulting ingot was homogenized at 350 °C for 48 h, followed by water quenching, then it was deformed using hot extrusion at 260 °C with an extrusion ratio of 36:1 at 1 mm/s. Samples with a diameter of 10 mm and a thickness of 3 mm were cut perpendicular to the extrusion direction. All the samples were ground to 2000 grit with SiC, followed by ultrasonically cleaning in acetone, absolute ethanol, and distilled water.

2.2. Double Substituted with Manganese and Strontium Tricalcium Phosphate Powder and Disc Preparation and Characterization

Double substituted phosphates were synthesized using a high-temperature solid-state reaction at 1200 $^{\circ}$ C (1):

$$2.8 CaO + 0.1 Sr(NO_3)_2 + 0.1 Mn(CH_3COO)_2 + 2(NH_4)_2 HPO_4 \rightarrow Ca_{2.8} Sr_{0.1} Mn_{0.1}(PO_4)_2 + 4NH_3 \uparrow + 0.2NO_2 \uparrow + 0.2CH_3COOH \uparrow + 3H_2O \uparrow$$
 (1)

All reagents were of analytical grade. Before sintering, all components (calcium oxide, strontium nitrate, manganese acetate), taken in the quantities according to the reaction 1 (14 g (0.25 mol) calcium oxide, 5.25 g (0.025 mol) strontium nitrate, 4.35 g (0.025 mol) manganese acetate), were mixed in a planetary mill with zirconia balls at a ratio of materials:balls = 1:5 at a speed of 1500 rpm. The duration of the heat treatment at 1200 °C was

Coatings 2023, 13, 36 4 of 13

4 h. The heating rate was 10 °C/min. After sintering, the samples were crushed, and after that, the powder was ground in a planetary mill with a rotation speed of about 1500 rpm for 30 min. After grinding, the powder was pressed into discs with a diameter of 20 mm and fired again at 1200 °C for 4 h. After that, the discs were crushed again, as described above. This procedure was repeated four times.

Further, the final discs were obtained from the prepared powder with two-sided uniaxial pressing at a specific pressure of 100 MPa/cm². The discs were kept in a chamber furnace with silite heaters at 1200 °C for 2 h.

The X-ray diffraction spectra of powder samples were recorded using an Ultima IV Rigaku X-ray diffractometer (Tokyo, Japan) with a vertical goniometer and a D/teX high-speed semiconductor detector. The investigation was conducted using CuK α radiation in the range of angles $2\theta = 9^{\circ}-100^{\circ}$ with a step of 0.02° . The detector movement speed was 2° /min. The phase analysis of spectra was carried out using the ICDD database and Sleve software.

For elemental analysis of the powder, atomic absorption spectroscopy (AAS) was applied. The analysis was carried out with AAS from Thermo Fisher Scientific, model iCE 3000 (Waltham, MA, USA).

The microstructure of the powder samples was investigated using a scanning electron microscope (SEM) (Tescan Vega II, Brno, Czech Republic) with an energy-dispersive X-ray (EDX) spectrometer. The acceleration voltage of the electron gun was 17–21 kV. The distribution of Mn and Sr ions in the powder was investigated using EDX analysis with the INCA Energy 300 energy dispersive microanalysis system (Oxford Instruments, Oxford, UK).

2.3. Pulsed Laser Deposition and Characterization of Coatings

Mn,Sr-TCP discs were used as targets for thin film deposition onto Zn-Li substrates and monocrystalline (100) silicon (Si) using the nanosecond PLD technique. Deposition experiments were carried out using an Nd:YAG laser source (532 nm, 10 Hz, 7 ns) focused by means of a 350 mm quartz lens in a stainless steel vacuum chamber. The chamber was evacuated at the pressure of 4×10^{-4} Pa by means of a vacuum system formed by scrool/turbomolecular vacuum pumps. Coatings were deposited at room temperature in the presence of O_2 at the pressure of 10 Pa, the fluence of 12 J/cm² for the deposition time of 3 h, and with a target–substrate distance of 1 cm. During the experiments, the disc target was kept in a rotating holder in order to minimize the laser-damaging craterization effect. Coatings deposited on Si substrates were used for FTIR and XRD characterizations.

The phase composition of the target and films was investigated using X-ray diffraction (Siemens 5000D, Bruker, Billerica, MA, USA) operating at 40 kV and 32 mA and using $\text{CuK}\alpha$ radiation.

The composition of the films was characterized with FTIR spectroscopy (Jasco 460 Plus, Jasco, Tokyo, Japan) operating with a resolution of 4 cm⁻¹ and X-ray photoelectron spectroscopy (XPS, PHOIBOS 100-MCD5 Specs spectrometer, SPECS GmBH, Berlin, Germany) equipped with a polychromatic Mg K α radiation. XPS spectra for each element were acquired with a channel width of 0.1 eV, and element peaks were deconvoluted with Voigt functions by using Google software, which allowed us to evaluate the intrinsic and extrinsic features of the XPS spectra. Peak positions were referenced to the C1s aliphatic carbon contribution set at 285.0 eV.

The morphology of the film surface was studied using Scanning Electron Microscopy (SEM, ESEM XL30-FEI, Philips, North Billerica, MA, USA).

2.4. Antimicrobial Activity Tests

Gram-positive (*S. aureus, E. faecalis*) and Gram-negative (*S. typhimurium, E. coli*) bacteria strains and *C. albicans* fungus were used to test the antimicrobial activity of the Mn,Sr-TCP-coated Zn-Li alloys. First, the coated Zn-Li substrates were UV sterilized for 30 min and immersed in 5 mL of Brain Heart Infusion (BHI, DIFCO, Sparks, NV, USA)

Coatings 2023, 13, 36 5 of 13

containing the individual microorganisms. Positive control tests were set up by growing the organisms in BHI. All organisms were grown under slow agitation for 24 h at their respective optimum growth temperatures. In particular, the bacteria (*S. aureus, E. coli, S. typhimurium,* and *E. faecalis*) were grown at 37 °C, while the fungus (*C. albicans*) at 28 °C.

The growth of microorganisms in the absence and in the presence of Mn,Sr-TCP-coated Zn-Li alloys was evaluated by reading the optical density at a wavelength of 600 nm (OD600) with a Biophotometer D30 (Eppendorf, Hamburg, Germany). The experiments were carried out in triplicate, and the results were expressed as the mean of the OD600 and the relative standard deviation (SD). The growth (in%) was calculated using the A/B × 100 equation, whereas the % of inhibition was calculated from (B – A)/B × 100 (where A and B, respectively, represent the mean of the OD600 of the microbial suspension with and without Mn,Sr-TCP-coated Zn-Li samples). The statistical significance was evaluated using a two-tailed Student's t-test performed for each sample group.

3. Results and Discussion

According to the obtained XRD data, the prepared powder was composed mainly of β -TCP Ca₃(PO₄)₂ [01-073-4869 ICDD] and a small amount of a secondary phase of calcium pyrophosphate-Ca₂P₂O₇ [01-073-0440 ICDD], about 3 wt% (see Figure 1).

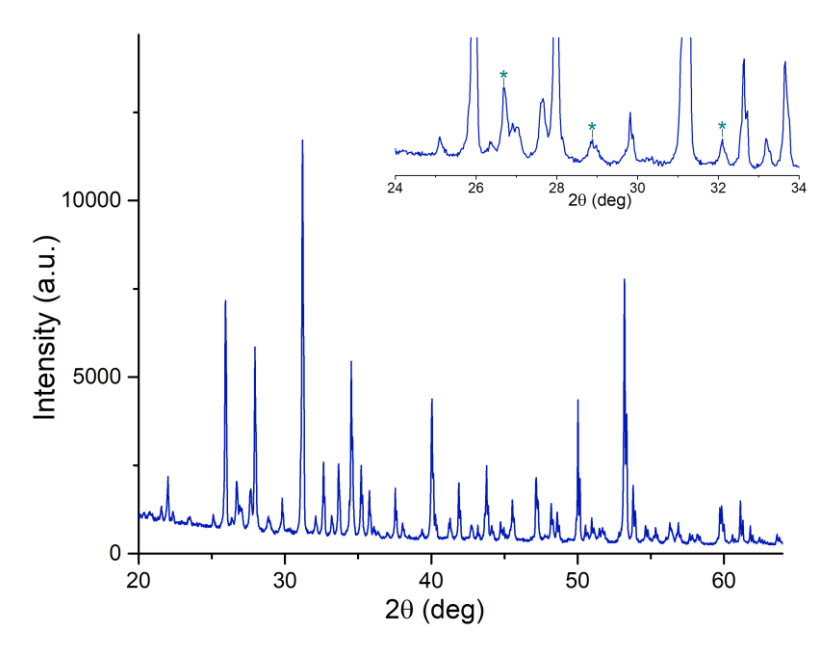


Figure 1. Experimental XRD pattern collected on Mn,Sr-TCP powder: β-TCP [01-073-4869 ICDD]. In the insert, the low-intensity region within the angular range of 24°–34° is highlighted. The peaks assigned to Ca₂P₂O₇ [01-073-0440 ICDD] secondary phase are marked with asterisks.

The Rietveld analysis of powder diffractograms was performed using the Jana 2006 program. The parameters of the crystal lattice were calculated as follows: for the undoped β -TCP, a = 10.338(6) Å, c = 37.401(5) Å; for Mn,Sr- β -TCP, a = 10.363(8) Å, c = 37.265(9) Å. A change in the crystal lattice parameters is an indication of replacing Ca atoms in the β -TCP lattice with Mn and Sr atoms, as it was also described for other substitution ions [37]. Lattice distortions may occur due to the difference in the ionic radii of Ca, Mn, and Sr; the value of the ionic radii for Ca²⁺ is 0.99 Å, for Mn²⁺- 0.46 Å, and for Sr²⁺- 1.13 Å.

The XRD pattern of the target presents all the signals of the β -TCP phase. No peaks attributable to other calcium phosphate phases were registered (see Figures 1 and 2a). The spectrum of the film deposited on the Si substrate is characterized by a broad band suggesting its low crystallinity (see Figure 2b). On the broad background, two main diffraction peaks can be distinguished at 2θ = 30.9 and 34.5, corresponding to the highest intensity peaks of the target, attributable to β -TCP [01-073-4869 ICDD].

Coatings 2023, 13, 36 6 of 13

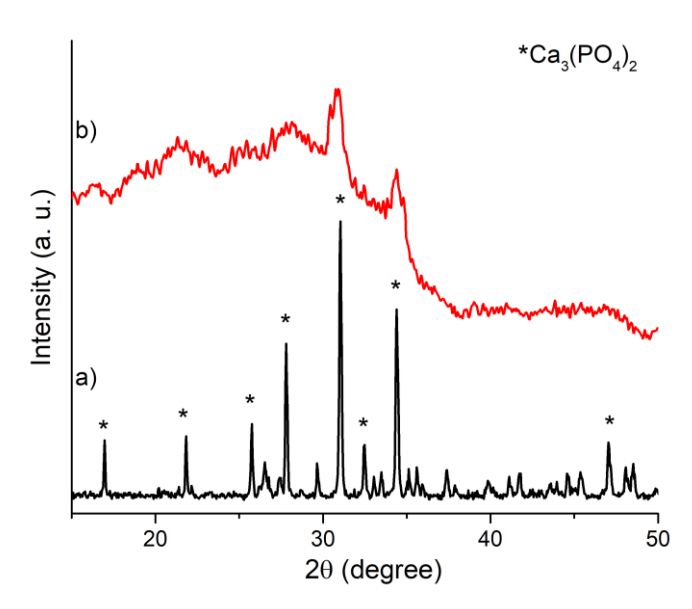


Figure 2. XRD patterns of (a) Mn,Sr-TCP target and (b) Mn,Sr-TCP coating deposited on Si.

In Figure 3, the FTIR spectra of the target and coatings are presented. In the FTIR spectrum of the target (Figure 3a), it is possible to observe typical β -TCP features. All signals are related to the PO₄3- group; peaks at 549 and 598 cm⁻¹ can be referred to as the ν_4 bending mode, peaks at 935 and 984 cm⁻¹ to the ν_1 symmetrical stretching mode, and peaks at 1012, 1025, and 1120 cm⁻¹ to the ν_3 anti-symmetrical stretching mode, respectively. The shift of each band with respect to the respective signal of pure β -TCP can be related to Mn and Sr substitutions. In the spectrum of the film deposited on Si, the two phosphate ν_4 bending modes converge in a single band, suggesting the low crystallinity of the composite films. Moreover, low-intensity signals at 1420 and 1500 cm⁻¹ suggest the formation of a small amount of carbonated calcium phosphate, which is typical for the PLD deposition procedure.

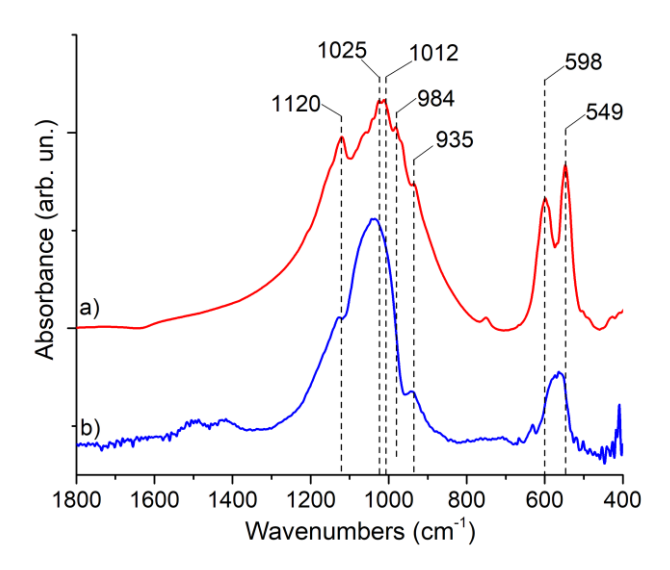


Figure 3. FTIR spectra of (a) Mn,Sr-TCP target and (b) Mn,Sr-TCP coating deposited on Si.

The film surface composition was studied using XPS analysis, and the results are presented in Table 1 and Figure 4. Signals of C 1s, O 1s, Ca 2p, P 2s, Mn 2p, and Sr 3p, characteristic of Mn,Sr-TCP composition, were observed. The presence of C1s was mainly due to impurities on the film's surface; however, the C1s component at B.E. of 288.8 eV can be related to carbonated TCP, confirming the FTIR analysis data. The Ca2p_{3/2} peak at

Coatings 2023, 13, 36 7 of 13

BE of 347.2 eV can be related to Ca^{2+} ions bonded to phosphate groups, the P2s signal at 190.5 eV is characteristic of phosphorus atoms in a $(PO_4)^{3-}$ group, Mn 2p3/2 peak centered at 641.5 eV can be related to Mn with a 2+ valence, and Sr 3p3/2 peak centered at 269.3 eV is related to Sr^{2+} .

Peak	B.E. (eV)	Assignment	
	285.0 eV	C aliphatic	
C 1s	286.6 eV	C-O	
	288.8 eV	CO ₃ 2-	
Sr 3p	269.3 eV	$Sr^{2+} 3p_{3/2}$	
	279.5 eV	$Sr^{2+} 3p_{1/2}$	
	347.2 eV	CaCO ₃ /Ca ₃ (PO ₄) ₂ 2p _{3/2}	

CaCO₃/Ca₃(PO₄)₂ 2p_{1/2}

 $Mn^{2+} 2p_{3/2}$

 $Mn^{2+} 2p_{1/2}$

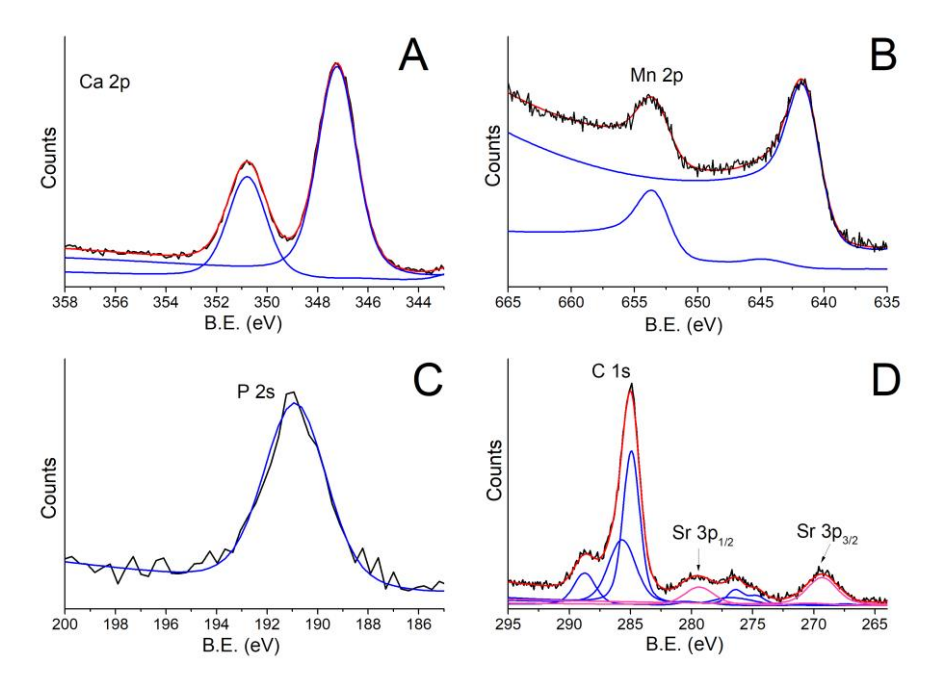
Ca₃(PO₄)₂

Table 1. XPS analysis results obtained for Mn,Sr-TCP coating.

Ca 2p

Mn 2p

P 2s



350.87 eV

641.56 eV

653.46 eV

190.5 eV

Figure 4. XPS spectra of Mn,Sr-TCP coating deposited on Zn-Li alloy: (**A**) Ca2p; (**B**)Mn2p; (**C**) P2s; (**D**)C1s-Sr2p . In the figure, black, red and blue lines represent the experimental data, the fitting curves and the peak components, respectively.

Mn,Sr-TCP powder is characterized by coarse granules with sizes ranging from tens to hundreds of microns (see Figure 5). The highest magnification allows the individuation of finer particles on the surface of coarse granules. The finest particulate size ranges from hundreds of nanometers to a few microns. The SEM-EDX analysis proved the presence of Mn and Sr and a homogeneous distribution of all the elements in the prepared Mn,Sr-TCP powder (see Figure 6).

Coatings 2023, 13, 36 8 of 13

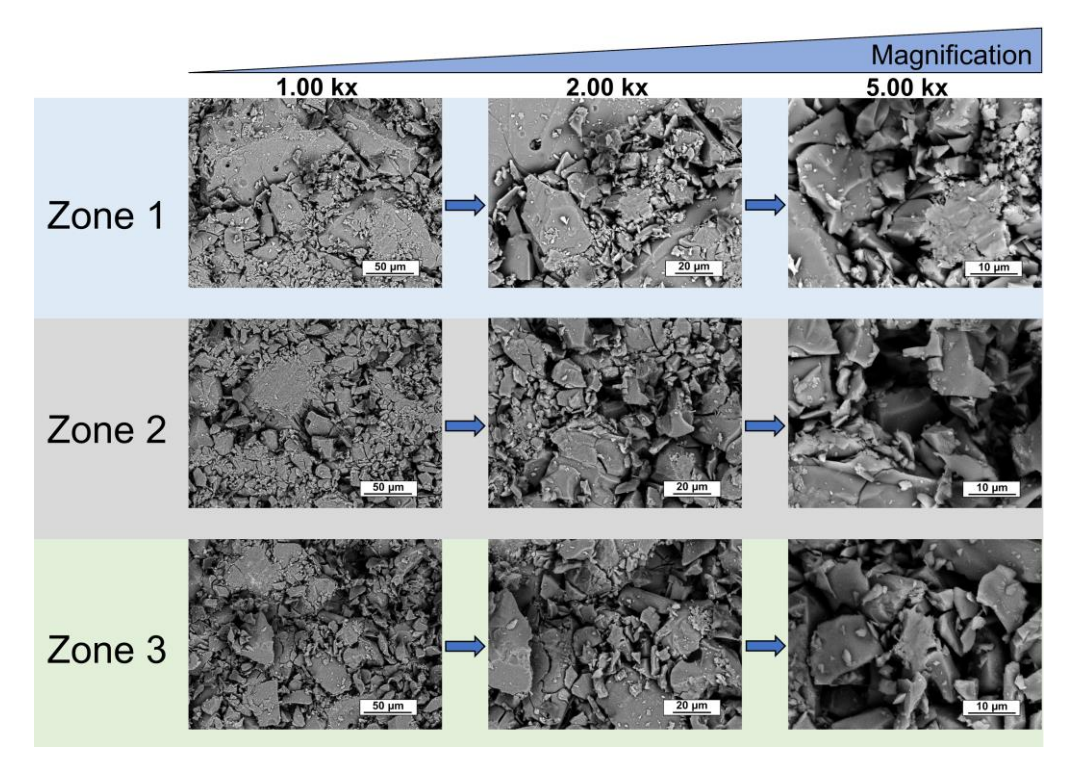


Figure 5. SEM images of different zones of Mn,Sr-TCP powder at various magnifications.

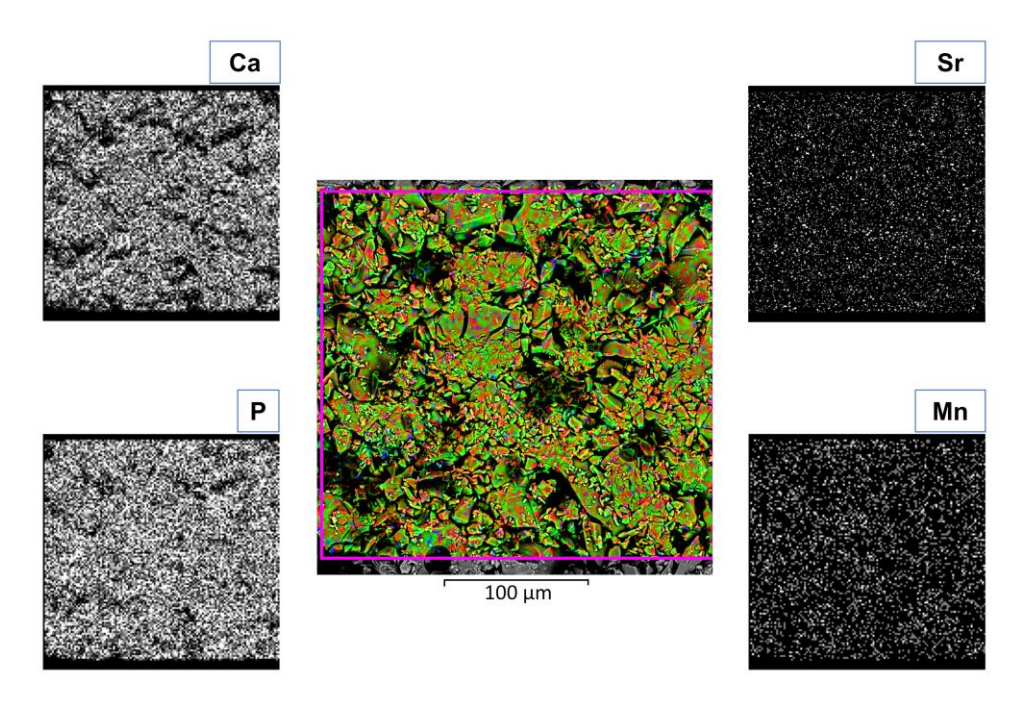


Figure 6. SEM-EDX composition of Mn,Sr-TCP powder.

The EDX, AAS, and calculated data on the content of Mn and Sr in the prepared powder are given in Table 2. There is a rather good agreement between the data obtained by different techniques, considering that the EDX method gives precise results only for polished samples, but, in our case, due to the relatively large roughness of the surface, the error in determining with the EDX method increased.

Table 2. Mn and Sr content in Ca2.5Mn0.25Sr0.25(PO4)2 powder.

Mn Conter	nt, wt.%	Sr Content, wt%	

Coatings 2023, 13, 36 9 of 13

EDX Data	AAS Data	Calculated	EDX Data	AAS Data	Calculated
3.77	4.65	4.29	6.53	6.45	6.75

Films deposited on Si substrates were uniform and compact, with round and irregularly shaped microparticles resting atop the nanostructured background (see Figure 7A–C). The presence of the gas buffer (O₂) in the deposition chamber and a short target substrate distance (1 cm) led to the confinement of the laser-induced plasma and promoted nucleation and growth of clusters and nanoparticles. Moreover, plasma confinement supported the growth of crystalline domains, transforming the diffuse contour of amorphous particles to sharp-edged ones. Surface characterization of Mn,Sr-TCP coating deposited on Zn-Li alloy is reported in Figure 7D–F. It is characterized by a uniform nanotextured background with globular-shaped particles on it (10 kx image). Some particles underwent coalescence, resulting in flattened round structures up to a few microns. Images collected at higher magnifications (50 and 100 kx) revealed that globular-shaped particles have a size distribution ranging from tenths of nanometers up to few microns and are randomly distributed on the surface.

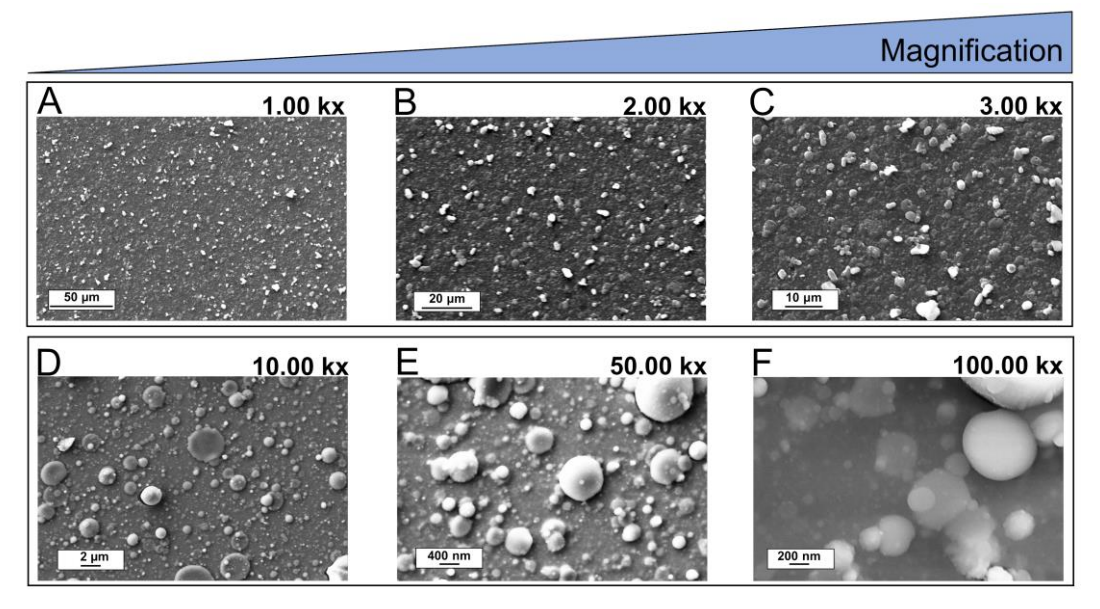


Figure 7. SEM images of Mn,Sr-TCP coating deposited on Si (A-C) and on Zn-Li (D-F) alloy.

The growth of microorganisms (*S. aureus, E. coli, S. typhimurium, E. faecalis,* and *C. albicans*) in the presence and absence of Mn,Sr-TCP-coated Zn-Li samples are detailed in Figure 8. In Figure 8, the percentage of growth and the percentage of inhibition derived from three independent experiments are given. The growth of each organism was evaluated after 24 h of incubation at respective optimal growth temperatures.

Coatings 2023, 13, 36 10 of 13

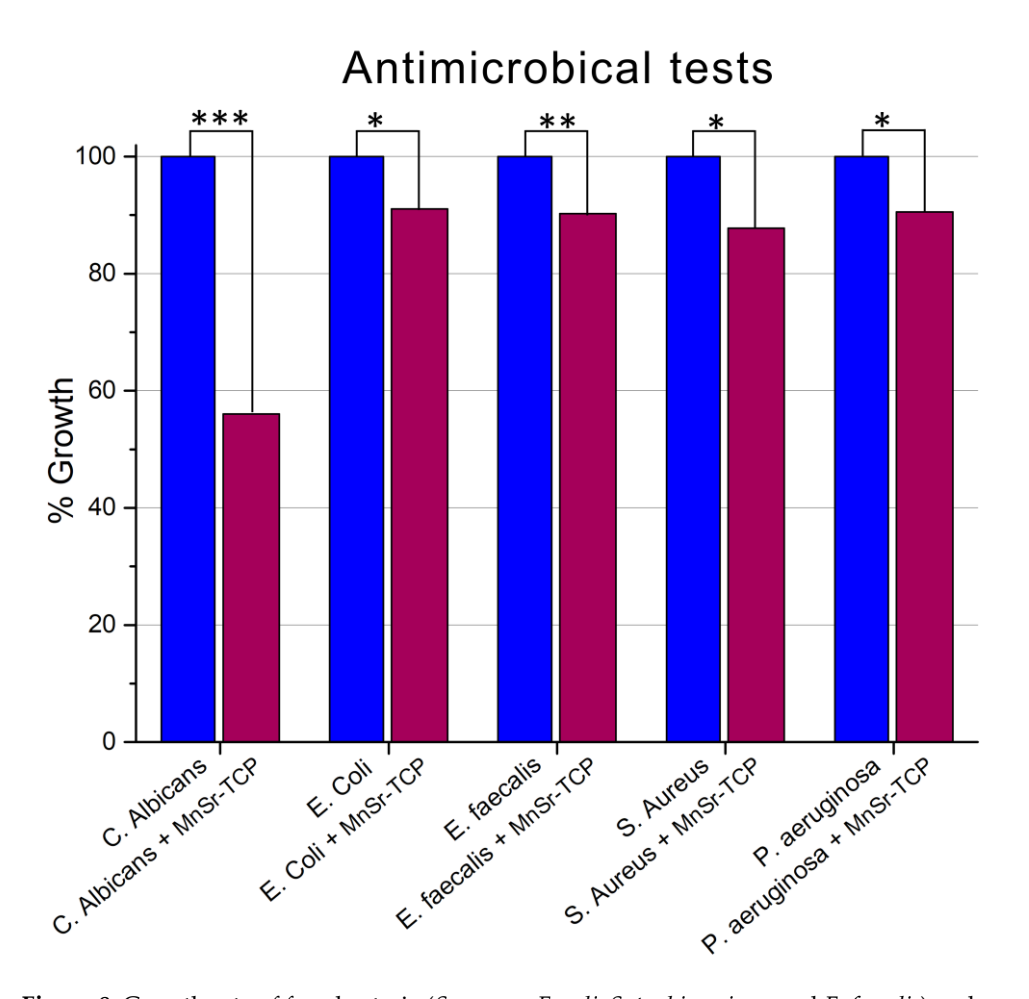


Figure 8. Growth rate of four bacteria (*S. aureus, E. coli, S. typhimurium*, and *E. faecalis*) and one fungus (*C. albicans*) grown in the presence and absence of Mn,Sr-TCP Zn-Li samples. The percentage of growth is calculated from three independent experiments. Statistical significance is reported for each bacterial group: *** (p < 0.001), ** (p < 0.01), * (p < 0.05).

For all the microorganisms, inhibition of growth was registered: a minimum of 8.95% for *E. coli* and a maximum of 43.96% for *C. albicans*. The other microorganisms have a very similar % of inhibition, in particular, for *P. aeruginosa*, 9.44%; *E. faecalis*, 9.74%; and *S. aureus*, 12.16%.

It should be mentioned that the bulk Mn,Sr- β -TCP composition exhibited more pronounced antimicrobial properties [26], which is likely connected to the fact that in the bulk, more antibacterial material is available.

To the best of our knowledge, there are only very few literature references regarding Mn,Sr-TCP. One of them is our previous work on various double substitutions of Ca²+ ions in TCP, among them Mn,Sr-TCP powder, its structural characterization and antimicrobial properties [26] mentioned above, and one other [38], describing MnSr-doped brushite bone cement. The authors [38] concluded that the properties of the cement depend on ionic substitutions, and the co-doping results in more benefits compared to single-doping, fostering the biological activity and, namely, the proliferation of human MG63 osteoblastic cells, their growth, and collagen secretion. The authors also suppose that Mn addition may be a promising way to improve the osteointegration of brushite cement *in vivo*. The authors [25] report on electrodeposited Mn,Sr-HA coating on commercially pure Ti. Excellent biocompatibility of the coating was attributed to a probable effect of both good surface wettability and release of Sr²+ and Mn²+ ions.

4. Conclusions

Coatings 2023, 13, 36 11 of 13

Double substituted with manganese and strontium TCP coatings on Zn-Li biodegradable alloys were deposited for the first time. The coating's main phase β -TCP was confirmed by the XRD and FTIR techniques. The XPS and SEM-EDX confirmed the presence of Mn and Sr. According to the XRD and FTIR data, low crystallinity coatings were deposited. The Mn,Sr-TCP coatings were compact and uniform, characterized by a nanostructured background and microparticles on the surface, typical for PLD deposition.

The antimicrobial activity test showed that Mn,Sr-TCP-coated Zn-Li alloys were able to inhibit the growth of all five microorganisms. In particular, the inhibition of 12.16% of *S. aureus*, 9.74% of *E. faecalis*, 9.44% of *P. aeruginosa*, and 8.95% of *E. coli* was registered. The Mn,Sr-TCP-coated Zn-Li alloys were very effective in inhibiting the growth of *C. albicans* fungus (about 50%). The prepared coatings can be useful in improving the degradation behavior and biological characteristics of Zn-Li alloys, and further investigation is needed before clinical translation.

Author Contributions: Conceptualization: J.V.R., A.D.B. and Y.Z.; Formal analysis: J.V.R., A.D.B., R.T., M.C., I.V.F., K.B. and M.F. Investigation: A.D.B., M.C., I.V.F., K.B., M.D.M.D.B. and M.F.; Methodology: J.V.R., A.D.B., R.T., I.V.F., K.B. and Y.Z.; Funding acquisition: J.V.R. and Y.Z. Supervision: J.V.R.; Writing—original draft: J.V.R.; Writing—review and editing: J.V.R. All authors have read and agreed to the published version of the manuscript.

Funding: J.V.R. and Y.Z. thank the bilateral project CNR (Italy)—NSFC (China) 2021–2022 and the International Cooperation and Exchange program of NSFC-CNR (Grant No. 52011530392).

Institutional Review Board Statement: Not applicable

Informed Consent Statement: Not applicable

Data Availability Statement: All data that support the findings of this study are included within the article.

Acknowledgments: The technical support of Marco Ortenzi and Luca Imperatori is gratefully acknowledged.

Conflicts of Interest: The authors declare no conflict of interest.

References

- Zheng, Y.F.; Gu, X.N.; Witte, F. Biodegradable metals. Mater. Sci. Eng. R 2014, 77, 1–34. https://doi.org/10.1016/j.mser.2014.01.001.
- 2. Windhagen, H.; Radtke, K.; Weizbauer, A.; Diekmann, J.; Noll, Y.; Kreimeyer, U.; Schavan, R.; Stukenborg-Colsman, C.; Waizy, H. Biodegradable magnesium-based screw clinically equivalent to titanium screw in hallux valgus surgery: Short term results of the first prospective, randomized, controlled clinical pilot study. *Biomed. Eng. Online* **2013**, *12*, 62. https://doi.org/10.1186/1475-925X-12-62.
- 3. Lee, J.W.; Han, H.S.; Han, K.J.; Park, J.; Jeon, H.; Ok, M.R.; Seok, H.K.; Ahn, J.P.; Lee, K.E.; Lee, D.H.; et al. Long-term clinical study and multiscale analysis of in vivo biodegradation mechanism of Mg alloy. *Proc. Natl. Acad. Sci. USA* **2016**, *113*, 716–721. https://doi.org/10.1073/pnas.1518238113.
- 4. Zhang, Z.; Jia, B.; Yang, H.; Han, Y.; Wu, Q.; Dai, K.; Zheng, Y. Biodegradable ZnLiCa ternary alloys for critical-sized bone defect regeneration at load-bearing sites: *In vitro* and *in vivo* studies. *Bioact Mater.* **2021**, *6*, 3999–4013. https://doi.org/10.1016/j.bioactmat.2021.03.045.
- 5. Seo, H.J.; Cho, Y.E.; Kim, T.; Shin, H.I.; Kwun, I.S. Zinc may increase bone formation through stimulating cell proliferation, alkaline phosphatase activity and collagen synthesis in osteoblastic MC3T3-E1 cells. *Nutr. Res. Pract.* **2010**, *4*, 356–361. https://doi.org/10.4162/nrp.2010.4.5.356.
- 6. Moonga, B.S.; Dempster, D.W. Zinc is a potent inhibitor of osteoclastic bone resorption in vitro. *J. Bone Miner Res.* **2010**, *10*, 453–457. https://doi.org/10.1002/jbmr.5650100317.
- 7. Yang, H.; Jia, B.; Zhang, Z.; Qu, X.; Li, G.; Lin, W.; Zhu, D.; Dai, K.; Zheng, Y. Alloying design of biodegradable zinc as promising bone implants for load-bearing applications. *Nat. Commun.* **2020**, *11*, 401. https://doi.org/10.1038/s41467-019-14153-7.
- 8. Rau, J.V.; Antoniac, I.; Fosca, M.; De Bonis, A.; Blajan, A.I.; Cotrut, C.; Graziani, V.; Curcio, M.; Cricenti, A.; Niculescu, M.; et al. Glass-ceramic coated Mg-Ca alloys for biomedical implant applications. *Mater. Sci. Eng. C Mater. Biol. Appl.* **2016**, *64*, 362–369. https://doi.org/10.1016/j.msec.2016.03.100.
- 9. Rau, J.V.; Antoniac, I.; Filipescu, M.; Cotrut, C.; Fosca, M.; Nistor, L.C.; Birjega, R.; Dinescu, M. Hydroxyapatite coatings on Mg-Ca alloy prepared by Pulsed Laser Deposition: Properties and corrosion resistance in Simulated Body Fluid. *Ceram. Intern.* **2018**, 44, 16678–16687. https://doi.org/10.1016/j.ceramint.2018.06.095.

Coatings 2023, 13, 36 12 of 13

Antoniac, I.; Miculescu, F.; Cotrut, C.; Ficai, A.; Rau, J.V.; Grosu, E.; Antoniac, A.; Tecu, C.; Cristescu, I. Controlling the Degradation Rate of Biodegradable Mg–Zn-Mn Alloys for Orthopedic Applications by Electrophoretic Deposition of Hydroxyapatite Coating. *Materials* 2020, 13, 263. https://doi.org/10.3390/ma13020263.

- 11. Antoniac, I.V.; Filipescu, M.; Barbaro, K.; Bonciu, A.; Birjega, R.; Cotrut, C.M.; Galvano, E.; Fosca, M.; Fadeeva, I.V.; Vadalà, G.; et al. Iron ion doped tricalcium phosphate coatings improve the properties of biodegradable magnesium alloys for biomedical implant application. *Adv. Mater. Interf.* **2020**, *7*, 2000531. https://doi.org/10.1002/admi.202000531.
- 12. Bohner, M.; Le Gars Santoni, B.; Döbelin, N. β-tricalcium phosphate for bone substitution: Synthesis and properties. *Acta Biomat.* **2020**, *113*, 23–41. https://doi.org/10.1016/j.actbio.2020.06.022.
- 13. Matsunaga, K.; Kubota, T.; Toyoura, K.; Nakamura, A. First-principles Calculations of Divalent Substitution of Ca(2+) in Trical-cium Phosphates. *Acta Biomater.* **2015**, *23*, 329–337. https://doi.org/10.1016/j.actbio.2015.05.014.
- Fadeeva, I.V.; Deyneko, D.V.; Forysenkova, A.A.; Morozov, V.A.; Akhmedova, S.A.; Kirsanova, V.A.; Sviridova, I.K.; Sergeeva, N.S.; Rodionov, S.A.; Udyanskaya. I.L.; et al. Strontium Substituted β-Tricalcium Phosphate Ceramics: Physiochemical Properties and Cytocompatibility. *Molecules* 2022, 27, 6085. https://doi.org/10.3390/molecules27186085.
- 15. Rau, J.V.; Fadeeva, I.V.; Forysenkova, A.A.; Davydova, G.A.; Fosca, M.; Filippov, Y.Y.; Antoniac, I.V.; Antoniac, A.; D'Arco, A.; Di Fabrizio, M.; Petrarca, M.; et al. Strontium Substituted Tricalcium Phosphate Bone Cement: Short and Long-Term Time-Resolved Studies and *In Vitro* Properties. *Adv. Mater. Interface* 2022, *9*, 2200803. https://doi.org/10.1002/admi.202200803.
- Fadeeva, I.V.; Lazoryak, B.I.; Davidova, G.A.; Murzakhanov, F.F.; Gabbasov, B.F.; Petrakova, N.V.; Fosca, M.; Barinov, S.M.; Vadalà, G.; Uskoković, V.; et al. Antibacterial and cell-friendly copper-substituted tricalcium phosphate ceramics for biomedical implant applications. *Mater. Sci. Eng. C Mater. Biol. Appl.* 2021, 129, 112410. https://doi.org/10.1016/j.msec.2021.112410. Epub 2021 Sep 2. PMID: 34579919.
- 17. Kazakova, G.; Safronova, T.; Golubchikov, D.; Shevtsova, O.; Rau, J.V. Resorbable Mg²⁺-Containing Phosphates for Bone Tissue Repair. *Materials* **2021**, *14*, 4857. https://doi.org/10.3390/ma14174857.
- 18. Rau, J.V.; Fadeeva, I.V.; Fomin, A.S.; Barbaro, K.; Galvano, E.; Ryzhov, A.P.; Murzakhanov, F.; Gafurov, M.; Orlinskii, S.; Antoniac, I.; et al. Sic Parvis Magna: Manganese-Substituted Tricalcium Phosphate and Its Biophysical Properties. *ACS Biomater. Sci. Eng.* **2019**, *5*, 6632–6644. https://doi.org/10.1021/acsbiomaterials.9b01528.
- Fadeeva, I.V.; Kalita, V.I.; Komlev, D.I.; Radiuk, A.A.; Fomin, A.S.; Davidova, G.A.; Fursova, N.K.; Murzakhanov, F.F.; Gafurov, M.R.; Fosca, M.; et al. In Vitro Properties of Manganese-Substituted Tricalcium Phosphate Coatings for Titanium Biomedical Implants Deposited by Arc Plasma. *Materials* 2020, 13, 4411. https://doi.org/10.3390/ma13194411.
- 20. Fadeeva, I.V.; Goldberg, M.A.; Preobrazhensky, I.I.; Mamin, G.V.; Davidova, G.A.; Agafonova, N.V.; Fosca, M.; Russo, F.; Barinov, S.M.; Cavalu, S.; et al. Improved cytocompatibility and antibacterial properties of zinc-substituted brushite bone cement based on β-tricalcium phosphate. *J. Mater. Sci. Mater. Med.* **2021**, *32*, 99. https://doi.org/10.1007/s10856-021-06575-x.
- 21. Dale, H.; Hallan, G.; Hallan, G.; Espehaug, B.; Havelin, L.I.; Engesaeter, L.B. Increasing risk of revision due to deep infection after hip arthroplasty. *Acta Orthop.* **2009**, *80*, 639–645. https://doi.org/10.3109/17453670903506658.
- 22. Zmistowski, B.; Karam, J.A.; Durinka, J.B.; Casper, D.S.; Parvizi, J. Periprosthetic joint infection increases the risk of one-year mortality. *J. Bone Jt. Surg. Am.* **2013**, *95*, 2177–2184.. https://doi.org/10.2106/JBJS.L.00789.
- 23. Moreira, M.P.; de Almeida Soares, G.D.; Dentzer, J.; Anselme, K.; de Sena, L.A.; Kuznetsov, A.; dos Santos, E.A. Synthesis of magnesium- and manganese-doped hydroxyapatite structures assisted by the simultaneous incorporation of strontium. *Mater. Sci. Eng. C Mater. Biol. Appl.* **2016**, *61*, 736–743. https://doi.org/10.1016/j.msec.2016.01.004.
- 24. Pina, S.; Canadas, R.F.; Jiménez, G.; Perán, M.; Marchal, J.A.; Reis, R.L.; Oliveira, J.M. Biofunctional Ionic-Doped Calcium Phosphates: Silk Fibroin Composites for Bone Tissue Engineering Scaffolding. *Cells Tissues Organs* **2017**, 204, 150–163. https://doi.org/10.1159/000469703.
- 25. Huang, Y.; Qiao, H.; Nian, X.; Zhang, X.; Zhang, X.; Song, G.; Xu, Z.; Zhang, H.; Han, S. Improving the bioactivity and corrosion resistance properties of electrodeposited hydroxyapatite coating by dual doping of bivalent strontium and manganese ion. *Surf. Coat. Technol.* **2016**, 291, 205–215. https://doi.org/10.1016/j.surfcoat.2016.02.042.
- 26. Deyneko, D.V.; Fadeeva, I.V.; Borovikova, E.Yu.; Dzhevakov, P.B.; Slukin, P.V.; Zheng, Y.; Xia, D.; Lazoryak, B.L.; Rau, J.V. Antimicrobial properties of co-doped tricalcium phosphates Ca_{3-x}(M'M")_x(PO₄)₂ (*Me* = Zn²⁺, Cu²⁺, Mn²⁺ and Sr²⁺). *Ceram. Intern.* **2022**, *48*, 29770–29781. https://doi.org/10.1016/j.ceramint.2022.06.237.
- 27. Schumacher, M.; Gelinsky, M. Strontium modified calcium phosphate cements—Approaches towards targeted stimulation of bone turnover. *J. Mater. Chem.* B. **2015**, *3*, 4626–4640. https://doi.org/10.1039/c5tb00654f.
- 28. Schumacher, M.; Wagner, A.S.; Kokesch-Himmelreich, J.; Bernhardt, A.; Rohnke, M.; Wenisch, S.; Gelinsky, M. Strontium substitution in apatitic CaP cements effectively attenuates osteoclastic resorption but does not inhibit osteoclastogenesis. *Acta Biomater.* **2016**, *37*, 184–194.. https://doi.org/10.1016/j.actbio.2016.04.016.
- Montesi, M.; Panseri, S.; Dapporto, M.; Tampieri, A.; Sprio, S. Sr-substituted bone cements direct mesenchymal stem cells, osteoblasts and osteoclasts fate. PLoS ONE 2017, 12, e0172100. https://doi.org/10.1371/journal.pone.0172100.
- 30. Braux, J.; Velard, F.; Guillaume, C.; Bouthors, S.; Jallot, E.; Nedelec, J.M.; Laurent-Maquin, D.; Laquerrière, P. A new insight into the dissociating effect of strontium on bone resorption and formation. *Acta Biomater.* **2011**, *7*, 2593–2603.. https://doi.org/10.1016/j.actbio.2011.02.013.
- 31. Aschner, M.; Erikson, K. Manganese. Adv Nutr. 2017, 8, 520–521. https://doi.org/10.3945/an.117.015305.
- 32. Bae, Y.J.; Kim, M.H. Manganese supplementation improves mineral density of the spine and femur and serum osteocalcin in rats. *Biol. Trace Elem. Res.* **2008**, 124, 28–34. https://doi.org/10.1007/s12011-008-8119-6.

Coatings 2023, 13, 36 13 of 13

33. Teghil, R.; Curcio, M.; De Bonis, A. Substituted Hydroxyapatite, Glass, and Glass-Ceramic Thin Films Deposited by Nanosecond Pulsed Laser Deposition (PLD) for Biomedical Applications: A Systematic Review. *Coatings* **2021**, *11*, 811. https://doi.org/10.3390/coatings11070811.

- 34. Neacsu, I.S.; Arsenie, L.V.; Trusca, R.; Ardelean, I.L.; Mihailescu, N.; Mihailescu, I.N.; Ristoscu, C.; Bleotu, C.; Ficai, A.; Andronescu, E. Biomimetic Collagen/Zn2+-Substituted Calcium Phosphate Composite Coatings on Titanium Substrates as Prospective Bioactive Layer for Implants: A Comparative Study Spin Coating vs. MAPLE. *Nanomaterials* **2019**, *9*, 692. https://doi.org/10.3390/nano9050692.
- 35. Kelly, R.; Miotello, A.; Mele, A.; Giardini Guidoni, A. Plume Formation and Characterization in Laser-Surface Interactions. In *Experimental Methods in the Physical Sciences*; Miller, J.C., Haglund, R.F., Eds.; Academic Press by Elsevier: Cambridge, MA, USA, 1997; Volume 30, pp. 225–289.
- 36. Perez, D.; Lewis, L.J.; Lorazo, P.; Meunier, M. Ablation of molecular solids under nanosecond laser pulses: The role of inertial confinement. *Appl. Phys. Lett.* **2006**, *89*, 141907. https://doi.org/10.1063/1.2358941.
- 37. Andronescu, E.; Predoi, D.; Neacsu, I.A.; Paduraru, A.V.; Musuc, A.M.; Trusca, R.; Oprea, O.; Tanasa, E.; Vasile, O.R.; Nicoara, A.I.; et al. Photoluminescent Hydroxylapatite: Eu³⁺ Doping Effect on Biological Behaviour. *Nanomaterials* **2019**, *9*, 1187. https://doi.org/10.3390/nano9091187.
- 38. Torres, P.M.C.; Marote, A.; Cerqueira, A.R.; Calado, A.J.; Abrantes, J.C.C.; Olhero, S.; da Cruz e Silva, O.A.B.; Vieira, S.I.; Ferreira, J.M.F. Injectable MnSr-doped brushite bone cements with improved biological performance. *J. Mater. Chem.* **2017**, *5*, 2017–2775. https://doi.org/10.1039/C6TB03119F.

Disclaimer/Publisher's Note: The statements, opinions and data contained in all publications are solely those of the individual author(s) and contributor(s) and not of MDPI and/or the editor(s). MDPI and/or the editor(s) disclaim responsibility for any injury to people or property resulting from any ideas, methods, instructions or products referred to in the content.